A&A 431, 183–195 (2005)
DOI: 10.1051/0004-6361:200400116

Astronomy & Astrophysics

Dust content in compact HII regions (NGC 7538-IRS1, IRS2, and IRS3)

K. Akabane and N. Kuno

Nobeyama Radio Observatory*, Minamimaki, Minamisaku, Nagano 384–1305, Japan
e-mail: kuno@nro.nao.ac.jp

Received 4 February 2003 / Accepted 13 September 2004

Abstract. The luminosity of the central star of the compact HII regions of NGC 7538 was estimated from the solid angle of the IR sources subtended relative to the central star, and was found to be 5 ∼ 10 times as intense as that of IR sources. Under the single central star approximation, the luminosity gives a stellar UV photon rate $N_{\rm U}(*)(s^{-1})$ of ∼3.0×10^{48}, ∼1.5×10^{49}, ∼5.1×10^{49}, and ∼1.7×10^{47} for the compact HII regions of NGC 7538-IRS1(A/2), B, IRS2, and IRS3, respectively. $N_{\rm U}(*)$ and the observed electron density, $n_{\rm e}$, provide the dust opacity of the ionizing photon, $\tau_{\rm Sd}$, for the optical path out to the Strömgren sphere radius $r_{\rm S}$, assuming a gas with standard dust content. Ionizing photon opacity over the same optical path but with the actual dust content $\tau_{\rm Sda}$ is also derived from $r_{\rm i}/r_{\rm S}$, where $r_{\rm i}$ is the radius of the ionized sphere, which is estimated from $N_{\rm U}(*)$ and the observed volume emission measure $n_{\rm e}^2(4\pi r_{\rm i}^3/3)$ (Spitzer 1978). An observational trend of $\gamma\{N_{\rm U}(*)/4\pi r_{\rm i}^2\}^{1/2}$ ∼ constant, where $\gamma = \tau_{\rm Sda}/\tau_{\rm Sd}$, was obtained for the 4 compact HII regions of the NGC 7538(N). Fourteen selected compact HII regions from data catalogued by VLA observations were examined for this trend, and a similar result was obtained. A limit of γ as $15 \geq \gamma \geq 0.1$ was given for the 14 selected sources. The size of the dust-depleted cavity of the NGC 7538(N) suggested by Chini et al. (1986) coincides with that of the ionized sphere of the IRS2 of the region.

Key words. HII regions – infrared: ISM – radio continuum: ISM – dust, extinction

1. Introduction

In this study, we try to find relations between dust content and certain parameters of compact HII regions. These relations, if any, should be understood in terms of the dust content in the compact HII regions.

Radio maps of compact HII regions were catalogued by Wood & Churchwell (1989), Kurtz et al. (1994), Dreher et al. (1984), Garay et al. (1993), Gaume et al. (1995a), De Pree et al. (1997) and Wood et al. (1988). Physical parameters of the compact HII regions were specified by Garay & Lizano (1999); compact HII regions have the electron density, $n_{\rm e}$, as $10^3 < n_{\rm e}\,({\rm cm}^{-3}) < 10^6$, diameter, D, as $0.001 < D({\rm pc}) < 0.5$, and the ionizing photon of the central star observed by radio, $N_{\rm U}$(radio), as $10^{44} < N_{\rm U}(s^{-1}) < 10^{50}$. Garay & Lizano (1999) concluded systematic trends for the relationship between ($n_{\rm e}$ and D), (EM and D), and ($N_{\rm U}$ and D), where EM denotes the emission measure as $n_{\rm e}^2\,D$. In this study, however, we would like to examine other relationships between the dust content of gas and the ionization parameters of the compact HII regions.

The procedure for estimating the dust content of gas from radio data is as follows: when the ratio (dust mass density)/(total mass density) is fixed as the specified standard gas, the proper intrinsic UV photon rate, $N_{\rm U}(*)$, and the observed electron destiny $n_{\rm e}$ yield dust opacity for the ionizing photon $\tau_{\rm Sd}$ with the optical path out to the Strömgren sphere radius, $r_{\rm S}$, (Spitzer 1978). The dust opacity for the ionizing photon along the same optical path $r_{\rm S}$, but of the gas actual dust content $\tau_{\rm Sda}$, is related directly to the ratio $r_{\rm i}/r_{\rm S}$ as given by Spitzer (1978), where $r_{\rm i}$ is the radius of the ionized sphere. $r_{\rm i}$ is estimated from the observed emission measure, $n_{\rm e}^2\,V$, where V is the volume of the ionized sphere, $V = 4\pi r_{\rm i}^3/3$, and $N_{\rm U}(*)$ the ionizing photon rate, assuming the recombination balance of electrons (Spitzer 1978). Then the ratio γ ($=\tau_{\rm Sda}/\tau_{\rm Sd}$) can be taken as a measure of actual dust content referring to that of the apparent standard gas, $\tau_{\rm Sd}$.

Near-infrared (NIR) observations of the NGC 7538(N) region were made by Campbell & Persson (1988) and Bloomer et al. (1998), and they found peculiarly weak emissions at 1.65 μm and 1.245 μm in the IRS1 region, respectively. Medium-infrared (MIR) observations of this region were made by Wynn-Williams et al. (1974, hereafter WBN), Werner et al. (1979) and Hackwell et al. (1982), for the multi-frequency spectrum and mapping observations. Some of them were accompanied by clear silicate absorption as seen in Willer (1976). Far-infrared (FIR) observations of the region were made by Werner et al. (1979), Thronson & Harper (1979), Chini et al. (1986) and IRAS. Recently, an 850 μm polarimetry

* Nobeyama Radio Observatory (NRO) is a division of the National Astronomical Observatory of Japan (NAOJ) under the National Institutes of Natural Sciences (NINS).

measurement has been made with the SCUBA of JCMT by Momose et al. (2001) and a 2 mm continuum observation was made by Akabane et al. (2001). Observations in CO (J = 1–0) (Kameya et al. 1989), CO (J = 3−2) (Kameya et al. 1991), ^{13}CO (J = 1–0) (Scoville et al. 1986) and CS (J = 2–1) (Kawabe et al. 1992) in the region revealed huge bipolar molecular out-flows around each region of IRS1, 9 and 11 of NGC 7538.

HII regions associated with NGC 7538-IRS1, 2 and 3 have small $r_{\rm i}$, ($0.002 < r_{\rm i}({\rm pc}) < 0.1$), and are known to be ultra-compact or compact. For the IRS1 region, radio observations by Campbell (1984), Campbell & Persson (1988) and Gaume et al. (1995b) revealed a strong bipolar structure of the source and identified the four components of the south sphere, the southern core, the northern core and the fourth component which seems to be visible near the northern core in the map by Gaume et al. (1995b, Figs. 1a and 1b). Northern and southern cores constitute a clear bipolar structure (Campbell 1984) as denoted by IRS1(A/2) × 2. The fourth component, as can be seen in the mm wave region, is the most intense component in the IRS1 region, which was predicted by Akabane et al. (1992) and Woody et al. (1989) from analyses of the observed intensity spectrum, as denoted by IRS1(B) in their work.

In the present study, we must know the fraction of $N_{\rm U}$(radio) to $N_{\rm U}(*)$ of the ionizing photon density emitted from the central star. For this, we use a method different from that of using IRAS luminosities. The total luminosity of the central star, $L_{*{\rm i}}$, which provides a proper $N_{\rm U}(*)$ with the assumption of the single star approximation (Panagia 1973) is estimated from the intrinsic luminosity of IR source, $L_{\rm IRSi}$, and its subtended solid angle to the central star. The IR sources are assumed to be located at around half the radius area of the ionized sphere, perhaps with an unfilled clumpy structure. IRAS data could not be used for the present study of $L_{*{\rm i}}$ because of too dense a concentration of the three IR sources. For the four sources, IRS1(A/2), (B), IRS2 and IRS3, we present a relationship such that $\gamma\{N_{\rm U}(*)/4\pi r_{\rm i}^2\}^{1/2} \sim$ constant.

Some sources which are catalogued by Wood & Churchwell (1989) and Kurtz et al. (1994) will be examined for this relationship. A limit of $0.1 \le \gamma \le 15$ was used for their data. Akabane & Kuno (2002) have reported a brief summary of this work.

2. IR source and central star

2.1. Luminosity of IR source

IRS1, 2, and 3 sources in the NGC 7538(N) region were observed by Wynn-Williams et al. (1974, WBN), Werner et al. (1979) and Hackwell et al. (1982). The total stellar luminosity, $L_{*{\rm i}}$ ($\simeq L_{\rm tot}$), is closely related to the intrinsic luminosity of IR sources, $L_{\rm IRSi}$, which are assumed to exist within each ionized sphere. Under the assumption of the single star approximation, $L_{*{\rm i}}$ gives the spectral type for ZAMS and then the intrinsic ionizing photon density, $N_{\rm U}(*)$, of the central exciting star (Panagia 1973). On the other hand, the absorption features with IR sources discovered by Gillet et al. (1975) and Willner (1976), and the transparency of the outside FIR dust (Akabane et al. 2001) may be useful to know the $L_{\rm IRSi}$. The dust layer

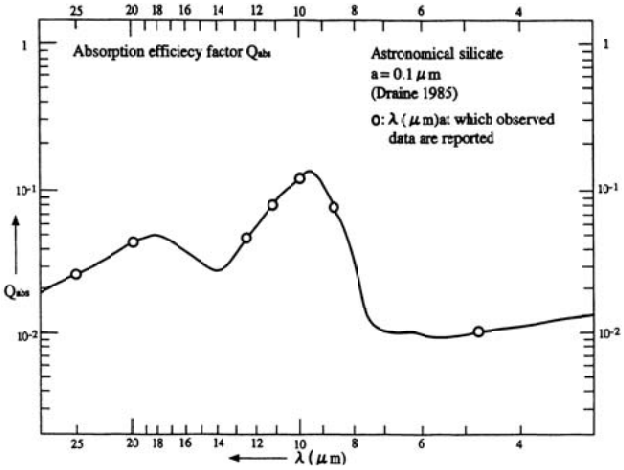

Fig. 1. Absorption efficiency factor $Q_{\rm abs}(\lambda)$ of astronomical silicate (Draine 1985) in the wavelength range of 4 μm to 25 μm.

Table 1. Efficiency factor for absorption applied with the grain of Willner's absorption dust layer. (i) Wavelength of reported observations: Wynn-Williams et al. (1974), Werner et al. (1977), and Hackwell et al. (1982). (ii) Efficiency factor for absorption of astronomical silicate with a radius of 0.1 (Draine 1985) (cf. Fig. 1).

λ (μm)$^{\rm (i)}$	$Q_{\rm abs}(\lambda)^{\rm (ii)}$
25	2.75
20	4.20
12.5	4.68
11.2	7.45
10.0	12.0
8.7	8.26
5.0	1.00
4.8	1.02

absorption will be examined again under the assumption that each IR source is an underlying black body located around the half radius area in the ionized sphere, following the study by Willner (1976) (cf. Fig. 6), and Beckwith et al. (1976). The absorption layer was assumed here simply to be made of grains of astronomical silicate such as presented by Draine (1985). The table of astronomical silicate in Draine (1985) gives the efficiency factor for absorption, $Q_{\rm abs}$, in a wide enough range of wavelengths, 4 μm−25 μm, around the peak at 9.7 μm (cf. Fig. 1 and Table 1). We see a quite similar wavelength dependence in the expected absorption feature of the IRS data by WBN and the absorption profile of Willner (1976) around the peak of $Q_{\rm abs}$ at 9.7 μm in Figs. 1 and 2. We can expect a broad band absorption dip at around the 10 μm range if the dust layer is reasonably thin and at a low temperature.

A simplified fundamental equation for the observed flux density of the IR source at frequency ν in the direction to the source (single beam area), S_ν, is given by,

$$S_\nu = B_\nu(T_{\rm IRS})\Omega_{\rm e}\exp\{-\tau_{\rm AS}(\lambda)\} + [1-\exp\{-\tau_{\rm AS}(\lambda)\}]B_\nu(T_{\rm AS})\Omega_{\rm B}, \quad (1)$$

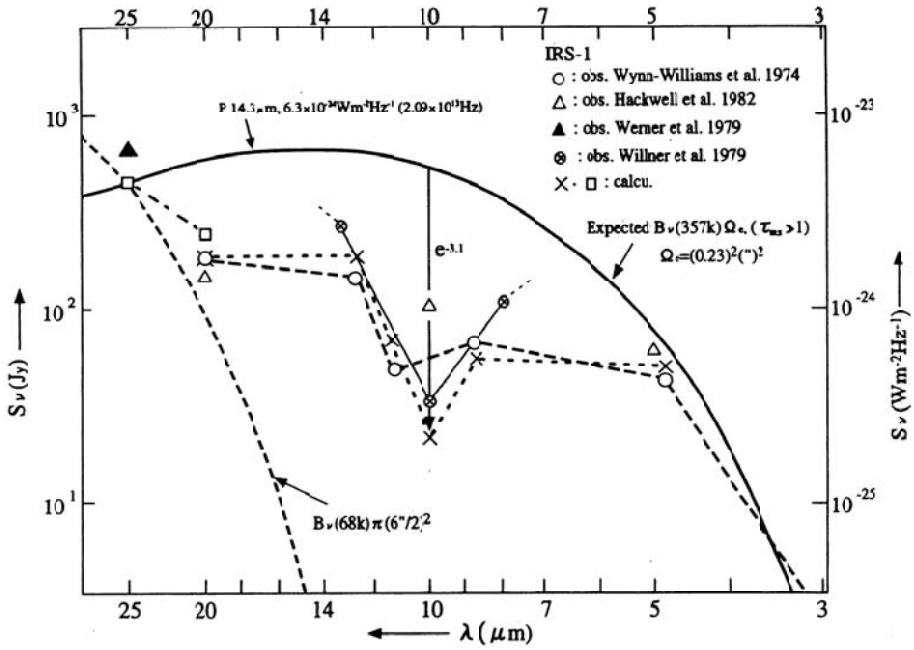

Fig. 2. Source IRS1 as an expected underlying black body with Willner's absorption layer.

Table 2. Expected underlying black body for IR sources. Column (1): Name of sources. (2): Peak flux density of the sources. (3): Wavelength at the peak of the fitting flux density. (4): Fitting temperature of the sources. (5): Effective solid angle of fitting source extension. (i): IRS1 with the data of Wynn-Williams et al. (1974). (ii): IRS1 with the data of Hackwell et al. (1982). (iii): Low temperature component of IRS2. (iv): High temperature component of IRS2.

Source	Peak flux density ($\mathrm{W\,m^{-2}\,Hz^{-1}}$)	λ(peak) (μm)	T_{IRS} (K)	Ω_{e} $(")^2$
(1)	(2)	(3)	(4)	(5)
IRS1[(i)]	6.3×10^{-24}	14.3	357	$(0.23)^2$
$\mathrm{IRS1_H^{(ii)}}$	3.0×10^{-24}	12.0	425	$(0.12)^2$
IRS2(L)[(iii)]	3.0×10^{-23}	46.4	110	$(2.9)^2$
IRS2(H)[(iv)]	1.2×10^{-24}	14.0	364	$(0.1)^2$
IRS3	1.3×10^{-24}	28.0	182	$(0.28)^2$

where $B_\nu(T_{\mathrm{IRS}})$, and $B_\nu(T_{\mathrm{AS}})$ are the Planck functions for the IR source of the temperature T_{IRS} and for the absorbing dust layer of the temperature T_{AS}. $\tau_{\mathrm{AS}}(\lambda)$ is the optical thickness of the absorbing dust layer at the wavelength λ. Ω_{e} and Ω_{B} are the net solid angle of the IR emission source and the equivalent solid angle of the observing beam width, respectively. In Eq. (1) we have assumed that $\tau_{\mathrm{IRS}} \gg 1$ for the IR source and $\Omega_{\mathrm{e}} \ll \Omega_{\mathrm{B}} \ll \Omega_{\mathrm{AS}}$, where Ω_{AS} is the solid angle of the extent of the absorbing dust layer. But, if the apparent (observed) extension of the IR source, Ω_0, is larger than Ω_{B}, S_ν of Eq. (1) must be integrated over the extension of brightness of the underlying black body, Ω_0, (e.g. for the case of IRS2 in this region). The first term of Eq. (1) corresponds to the flux density of the absorbed IR source, and the second term is that for the thermal emission of the absorbing dust layer.

For the study of the first term of Eq. (1), Fig. 2 shows an optimum fitting of $B_\nu(T_{\mathrm{IRS}})\Omega_{\mathrm{e}}$ (short dashed line). It was obtained by minimizing the differences between the observed flux density and that calculated from $B_\nu(T_{\mathrm{IRS}})\Omega_{\mathrm{e}}\exp\{-\tau_{\mathrm{AS}}(\lambda)\}$ in Eq. (1), assuming that the observed flux density at 20 μm is equal to the fitted one having τ_{AS} of 1.1. The value of $B_\nu(357\,\mathrm{K})(0.23'')^2$ is fixed as a probable approximation for IRS1, which turns out to be in good agreement with Willner's model of black body emissivity (Willner 1976). Werner et al. (1979) used both data observed by WBN & Willner (1976), and identified the 10 μm dip due to the absorption of silicate grains. For the second term of Eq. (1), we selected $B_\nu(68\,\mathrm{K})\pi(6''/2)^2$ in such a way that the thermal emission of the absorbing dust layer does not disturb the absorption of the first term and that its emission can explain, as well as possible, the rather intense 25 μm result of Werner (1979) which was observed with the beam width of $\pi(6''/2)^2$. Black body parameters of the IRS1 and the optical thickness $\tau_{\mathrm{AS}}(\lambda)$ for the absorbing dust layer, which are evaluated from the optimum fitting of $B(T_{\mathrm{IRS}})\Omega_{\mathrm{e}}$ as in Fig. 2, are listed in Tables 2 and 3. A mean error for the fitting point is estimated as $\langle\{1-(\tau_{\mathrm{AS}}/Q_{\mathrm{abs}})/\langle(\tau_{\mathrm{AS}}/Q_{\mathrm{abs}})\rangle\}^2\rangle = (\pm0.11)^2$.

Adopting the same procedure as in Fig. 2, we found no absorption layer for IRS2 (Fig. 3). It can be fitted by two almost absorption-free black bodies, $B_\nu(110\,\mathrm{K})(2.9'')^2$ for IRS2(L)

Table 3. τ_{AS} from the fitting to the observed data.

Source	4.8 μm	5.0 μm	8.7 μm	10.0 μm	11.2 μm	12.5 μm	20 μm	25 μm
IRAS1	0.29	–	1.7	–	2.1	1.2	1.1	–
$IRS1_H$	–	0.08	–	1.03	–	–	0.36	–
IRS2(L)				~0				–
IRS2(H)				~0				–
IRS3	–	–	–	0.76	–	–	0.26	–

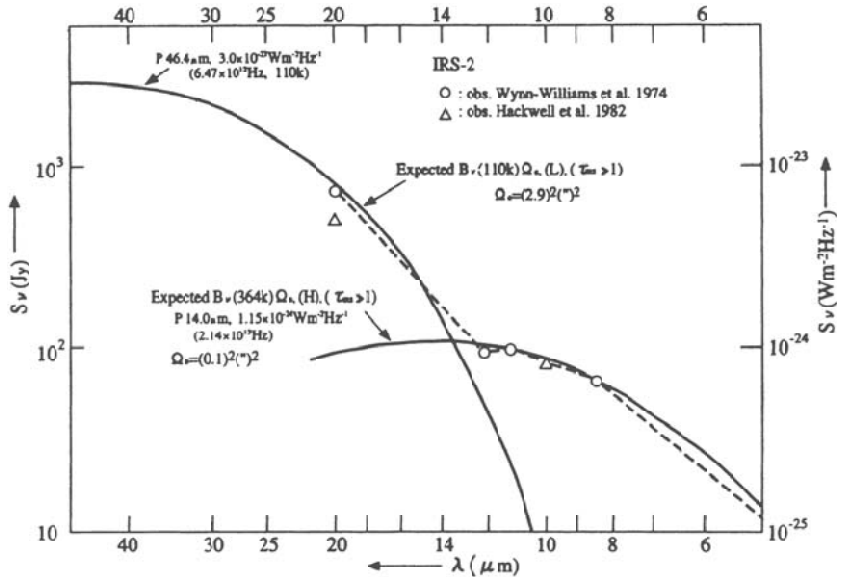

Fig. 3. Source IRS2 as an expected two black body structure of IRS2(L) and IRS2(H).

and $B_\nu(364\,\mathrm{K})(0.1'')^2$(H) for IRS2(H), as shown in Fig. 3. We estimated $B_\nu(T_{IRS})\Omega_e$ for IRS2(L) which provides the observed flux density at 20 μm, assuming that (1) this black body emission does not disturb the high temperature component of $B_\nu(364\,\mathrm{K})(0.1'')^2$(H) in the figure; (2) the effective size, Ω_e, of the IR source does not exceed that of the ionized sphere of $(7.6'')^2$ which was observed by Martin (1973) and Akabane et al. (1992); and (3) the red side wing of $B_\nu(T_{IRS})\Omega_e$ does not cover the extended dust emission of the NGC 7538(N) in the mm to sub-mm and FIR region. From some trials, $B_\nu(85\,\mathrm{K})(9.4'')^2$ seems to give the lower limit of temperature. $(9.4'')^2$ was estimated from the ratio of the expected flux density $B_\nu(85\,\mathrm{K})\Omega_e$ $(=S_\nu)$ to the corresponding brightness $B_\nu(85\,\mathrm{K})$. The effective size of the IR source with a temperature lower than 100 K may exceed that of the ionized sphere, and there is a possibility that the red side of flux density of the IR source may cover that of the extended dust in the mm to sub-mm range. Such confusion of flux densities has not been observed in this area so far (Akabane et al. 1992; ibid 2001). Therefore, we fixed the highest temperature of 110 K and then the smallest size of $(2.9'')^2$ for the IRS2(L) as in Fig. 3 and in Table 2. This also gives the minimum obscuration for L_{*i} of the central star by the IR source itself, which is ignored in this study. From these considerations, the expected luminosity of the central star L_{*i} for IRS2(L) was estimated to be $4.8\times10^5\,L_\odot$ (for $T_{IRS} = 85\,\mathrm{K}$) $< L_{*i} < 8.5\times10^5\,L_\odot$ (for $T_{IRS} = 110\,\mathrm{K}$). Willner (1976) did not find an absorption dip for IRS2, but he detected an NeII emission line at λ of 12.78 μm.

For IRS3, two wavelength data by WBN and two data by Hackwell et al. (1982) are available, and the underlying black body of $B_\nu(182\,\mathrm{K})(0.28'')^2$ is fairly well fitted, as shown in Fig. 4. The absorption dip of $\exp(-0.76)$ at around 10 μm is expected as in the figure, while Willner's absorption layer with a temperature lower than ~64 K will have no emission effect on the observed spectrum of the IR source as shown in the figure. Parameters of the black body and the silicate absorbing dust layer obtained are summarized in Tables 2 and 3, respectively. The mean error for the fitted two points is $\langle\{1-(\tau_{AS}/\tau_{abs})/\langle(\tau_{AS}/\tau_{abs})\rangle\}^2\rangle = (\pm0.012)^2$.

The intrinsic luminosity of the IR source, L_{IRSi}, is given using the Stefan-Boltzmann law as follows,

$$L_{IRSi} = \{1/(1-\eta)\}4R^2\Omega_e\sigma T_{IRS}^4, \quad (2)$$

where R (= 2.8 kpc) (Campbell 1984) denotes the adopted distance to the IR sources, σ the Stefan-Boltzmann constant, $(1-\eta)$ the fractional transparency through the clearance of the optically thick clumpy dust in the far outer region of the IR sources (cf. Fig. 6). For the present study, we assumed $\eta \sim 0.5$ as a probable working model (Akabane et al. 2001). New FIR imaging observations should clarify the structure of the dust in the far outer region. L_{IRSi} estimated for each IR source is listed in Col. 4 of Table 4. When we adopt the distance to the source

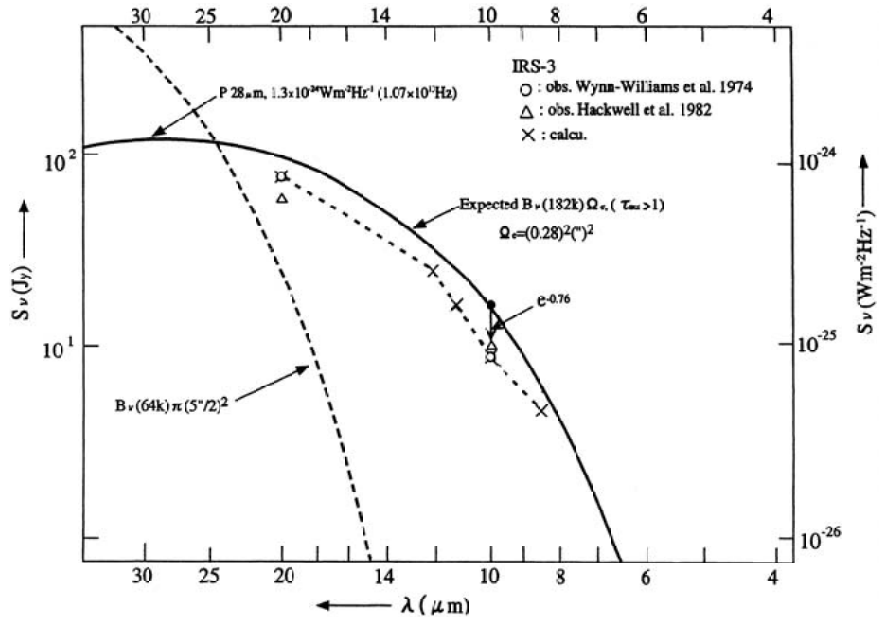

Fig. 4. Source IRS3 as an expected underlying black body with Willner's absorption layer.

as $R > 2.8$ kpc, we must consider the multiple star excitation model (Wood & Churchwell 1989, hereafter WC; and Garay et al. 1993) of the IRS2 for the required central star younger than O4 of the spectral type.

2.2. Location of IR source

The NMA 98 GHz result of the NGC 7538(N) is reproduced in Fig. 5 (Akabane et al. 1992) referring to the positions of IRS1, 2, and 3 by WBN. We see in the figure that IRS2 is in the radio contour map about 3″ (arca) from the radio center. Although this is not direct evidence that IRS2 is within the ionized region, we assume in this study that IRS2 is located at a radius of about 3″ in this ionized region. This assumption seems to be roughly supported in the case of IRS2, since the observed position and extent at 20 μm by WBN and those in radio maps by Martin (1973), Campbell & Persson (1988), Kameya (1992, 5 GHz, VLA, private communication) and Akabane et al. (1992) agree well for both with ∼7″ in diameter. The position of IRS1 is also shown in the radio map of Fig. 5. IRS1 and the radio peak (unresolved) coincide within ∼1″ of the probable observational error. The same situation for the positions of IRS1 and IRS3 is shown by WBN & Martin (1973), such that they coincide with those of each radio concentration within an observational error of ∼1″. Beckwith et al. (1976, Fig. 5) also showed the IR source to be within an HII region. Then, in this study we assumed that IRS1, IRS2 and IRS3 of NGC 7538(N) are located roughly at $r_{\rm IRS} = r_{\rm i}/2$ in each region, where $r_{\rm IRS}$ is the distance of the IR source from the center and $r_{\rm i}$ is the radius of the ionized sphere, as illustrated schematically in Fig. 6.

2.3. Luminosity of the central star

The luminosity of the central star, $L_{*\rm i}$, can be estimated from the intrinsic luminosity of IR sources, $L_{\rm IRSi}$, and the total solid

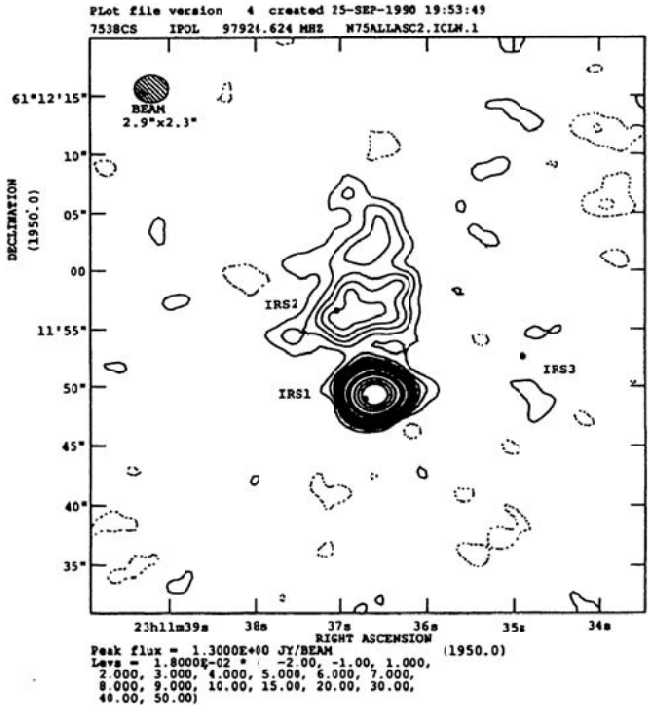

Fig. 5. 98 GHz contour map of the IRS1, 2 and 3 region by the NMA with the synthesis beam width of 2.9″ × 2.3″. The dots are for the positions of IRS1, 2, and 3, (Wynn-Williams et al. 1976).

angle subtended by IR sources to the central star (cf. Fig. 6). When we define $\Omega_0 = \pi r_{\rm i}^2/R^2$ (R is the distance to IRS) and $\Omega_{\rm e} = \pi a_{\rm I}^2/R^2$ ($a_{\rm I}$ is the radius of IRS), $(\pi a_{\rm I}^2/r_{\rm IRS}^2)/4\pi$ (= $L_{\rm IRSi}/L_{*\rm i}$), where $r_{\rm IRS} \sim r_{\rm i}/2$, is related by

$$L_{*\rm i} = (\Omega_0/\Omega_{\rm e})L_{\rm IRSi}. \quad (3)$$

IR sources are assumed to be located at around half a radius area in the ionized sphere. From $L_{*\rm i}$ in Eq. (3), assuming the single star approximation, we can derive the spectral type of

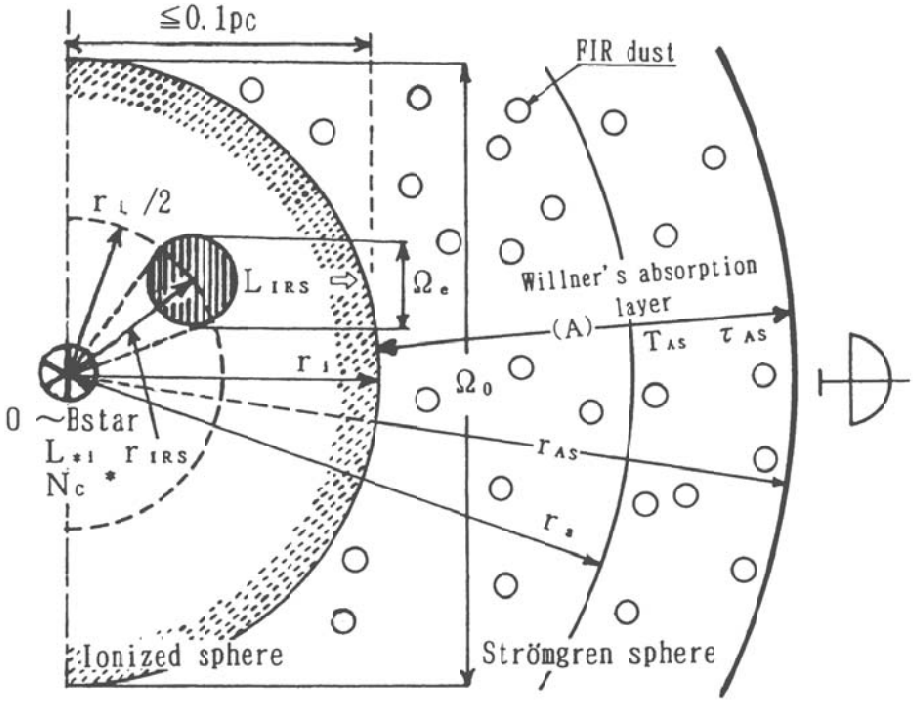

Fig. 6. A model structure of the compact or ultra-compact HII region.

the central star assumed to be on the ZAMS, which provides the stellar ionizing photon, $N_{\rm U}(*)$, (Panagia 1973 and Spitzer 1978).

The dust temperature $T_{\rm d}$ at radius $r_{\rm d}$ will be estimated from the stellar luminosity $L_{*{\rm i}}$, under the assumption of local thermodynamical equilibrium ($L_{*{\rm i}} = 4\pi r_{\rm d}^2 \times 4\sigma T^4$), as follows,

$$T_{\rm d}(r_{\rm d}) \simeq (L_{*{\rm i}}/16\pi\sigma)^{1/4} r_{\rm d}^{-1/2}. \quad (4)$$

Conversely, this equation can also be used to find the order of $r_{\rm d}$ for an appropriate dust temperature $T_{\rm d}$.

The total luminosity of IRS1, in Table 4, can possibly be separated into IRS1(A/2) × 2 and (B), which are in proportion to the ratio of each observed volume emission measure. Component (A) has a bipolar structure (Campbell 1984), and component (B) is from the work of Akabane et al. (1992) as the HII region of IRS1. The half radius of the ionized sphere of the component (A/2) (=1.3×10^{16} cm) is roughly taken to be $r_{\rm IRS}$ for IRS1 which gives $L_{*{\rm i}}$ in Eq. (3) including (A/2) × 2 and the nearby unresolved but more intense HII component (B) (Akabane et al. 1992). The estimated results are summarized in Table 4. The estimated parameters for the dust absorption layer (Willner 1976) are also listed in Table 4. The central distance of the layer, $r_{\rm AS}$, is derived from Eq. (4) with the required dust temperature $T_{\rm AS}$ in Figs. 2 and 4.

3. Dust content and ionizing photon density

3.1. Dust opacity out to Strömgren sphere radius

In the preceding section, the intrinsic ionizing photon rate of the single central star, $N_{\rm U}(*)$, has been estimated for the study of compact HII regions. The results are given in Col. 4 of Table 5 with the expected spectral type of central star. In this section, we study the dust opacity for ionizing photons out to the Strömgren sphere radius, following Spitzer (1978), Petrosian et al. (1972) and Vacca et al. (1996).

We follow the extinction criterion for the standard gas by Spitzer (1978; Eqs. (5)−(23)) that

$$(\tau_{\rm Sd}/\tau_{\rm SH}) = 1/3100, \quad (5)$$

where $\tau_{\rm Sd}$ and $\tau_{\rm SH}$ are the optical thicknesses of dust and atomic hydrogen respectively, for an ionizing photon from the central star over a path length identical to the Strömgren sphere radius, $r_{\rm S}$ (Spitzer 1978; Eqs. (5)−(21); and Vacca et al. 1996). From the definition of Eq. (5), if we know the actual electron density $n_{\rm e}({\rm cm}^{-3})$ of the region and the actual central UV photon rate $N_{\rm U}(*)({\rm s}^{-1})$, we can calculate an apparent optical thickness $\tau_{\rm Sd}$, assuming a standard gas (Eq. (5)) as follows:

$$\begin{aligned}\tau_{\rm Sd} &= (s/3100)\{3N_{\rm U}(*)/4\pi\alpha_{\rm B}\}^{1/3} n_{\rm e}^{1/3} \\ &= 1.65 \times 10^{-17} N_{\rm U}(*)^{1/3} n_{\rm e}^{1/3}, \end{aligned} \quad (6)$$

where s ($\simeq 6.3 \times 10^{-18}\,{\rm cm}^2$) is the ionizing photon absorption coefficient for a hydrogen atom in the $n = 1$ level, $\alpha_{\rm B}$ ($\simeq 4.5 \times 10^{-13}\,{\rm cm}^3\,{\rm s}^{-1}$) the recombination coefficient excluding captures to the $n = 1$ level for $T_{\rm e} = 5000$ K, and $n_{\rm e}({\rm m}^{-3})$ the observed electron density in the ionized region assuming $n_{\rm e} = n_{\rm H}$ (atomic hydrogen density) for fully ionized gas.

We consider now the radius $r_{\rm i}$ of the ionized gas, assuming that $\tau_{\rm Sd}$ is acceptable as the actual $\tau_{\rm Sda}$. Estimation of $r_{\rm i}$, the radius of the ionized sphere with the actual dust content, which has a sharp ionization boundary with the vanishing central ionizing photon at $r_{\rm i}$, can also be made from the calculation by Spitzer (1978; pp. 112−113). According to Spitzer (1978), writing $y = r/r_{\rm S}$ for the distance r from the central star,

Table 4. Parameters of IR sources and Willner's absorption dust layer. Column (3): Intrinsic luminosity of the central star under single star approximation. (4): Intrinsic luminosity of IR source. (5): Central distance of the IR source as $r_{\rm IRS} = (1/2)r_{\rm i}$, where $r_{\rm i}$ is radius of ionized sphere. (7): Observed solid angle of the ionized sphere. (9): Central distance of the absorption dust layer from Eq. (4) with $T_{\rm AS}$ of the required dust temperature. (10): Estimated temperature of the dust layer for absorption. (11): Opacity for the absorption by Willner's dust layer. (i) and (ii): A and B are symbols of the compact HII region component of IRS1 (Akabane et al. 1992). $L_{*{\rm i}}/L_\odot$ for each component must be shared from the total luminosity (A+B). (see the text) (iii): Turnover frequency of the free-free emission is taken at 5 GHz (Akabane et al. 1992).

Sources	Star		IRS ($\tau_{\rm IRS} \gg 1$)					Silicate dust layer for absorption		
(1)	(2)	(3)	(4)	(5)	(6)	(7)	(8)	(9)	(10)	(11)
NGC 7538	Spectral	$L_{\rm i}/L_\odot$	$L_{\rm IRSi}/L_\odot$	$r_{\rm IRS}$	$T_{\rm IRS}$	Ω_0	$\Omega_{\rm e}/\Omega_0$	$r_{\rm AS}$	$T_{\rm AS}$	$\tau_{\rm AS}$
(N)	type			(cm)	(K)	$('')^2$		(cm)	(K)	($10\,\mu$m)
IRS1(A/2)[(i)]	$\sim$O7 $\times$ 1	9.6×10^4	–	6.5×10^{15}	–	–	–	–	–	–
	(×2)	(×2)		(A/2)						
	–	5.2×10^4	8.65×10^4	6.5×10^{15}	357	$(0.55)^2$	5.7^{-1}	2.5×10^{17}	$\sim$68	3.1
		(A+B)	(A+B)	(A+B)	(A+B)	(A+B)	(A+B)	(A+B)		
IRS1(B)[(ii)]	$\sim$O6 $\times$ 1	3.2×10^5	–	1.9×10^{15}	–	–	–	–	–	
	(×1)	(×1)		(B)						
$\rm IRS1_H$	$\sim$O5 $\times$ 1	7.0×10^5	4.94×10^4	7.0×10^{15}	425	$(0.59)^2$	21^{-1}	$>3.6\times10^{17}$	<68	1.03
IRS2(L)	–	–	1.27×10^5	8.5×10^{16}	110	$(7.6)^2$	6.7^{-1}	–	–	–
	$\sim$O4.5 $\times$ 1	8.5×10^5								
IRS2(H)	–	–	1.61×10^4	6.0×10^{15}	364	$(0.51)^2$	$\sim34^{-1}$	–	–	–
IRS3[(iii)]	$\sim$B0 $\times$ 1	3.3×10^4	9.13×10^3	6.5×10^{15}	182	$(0.55)^2$	3.6^{-1}	$>0.7\times10^{17}$	<64	0.76

the optical thickness $\tau_{\rm Sda}$ for the gas of actual dust content is related to the Eqs. (5)−(29) in Spitzer (1978) as follows:

$$3\int_0^{y_i} y^2 \exp(y\tau_{\rm Sda})\,{\rm d}y = 1, \tag{7}$$

and the numerical table of $\tau_{\rm Sda}$ {$=\tau_{\rm Sd}$ in Spitzer (1978)} with $y_{\rm i}$ ($=r_{\rm i}/r_{\rm s}$) is shown (ibid; Tables 5−4).

On the other hand, the fractional ionizing photons of $N_{\rm U}(*)$, which are consumed by the ionization of hydrogen, $(r_{\rm i}/r_{\rm S})^3\,N_{\rm U}(*)$, is balanced by the number of electron recombinations within the ionized sphere as follows:

$$\begin{aligned}(r_{\rm i}/r_{\rm s}) &= \{\alpha_{\rm B}(n_{\rm e}^2\,V)/N_{\rm U}(*)\}^{1/3} \\ &= 7.66\times10^{-5}N_{\rm U}(*)^{-1/3}(n_{\rm e}^2\,V)^{1/3},\end{aligned} \tag{8}$$

where $n_{\rm e}^2\,V$ is the volume emission measure of the ionized sphere, and $V = 4\pi r_{\rm i}^3/3$. Then if we know $r_{\rm i}/r_{\rm s}$ ($=y_{\rm i}$) from an assumed $N_{\rm U}(*)$ and radio observed $n_{\rm e}^2\,V$, we can estimate the corresponding $\tau_{\rm Sda}$ graphically from the curve of the numerical table of $\tau_{\rm Sda}$ and $y_{\rm i}$ from Eq. (7) (Spitzer 1978).

Keeping the relative dust content at $\tau_{\rm Sda}/\tau_{\rm SH} = \tau_{\rm Sd}/\tau_{\rm SH} \equiv 1/3100$, both calculated dust opacities $\tau_{\rm Sd}$ from Eq. (6) and $\tau_{\rm Sda}$ from Eqs. (7) and (8) should coincide with each other for a certain value of $N_{\rm U}(*)$, from which we can also estimate the total luminosity and the spectral type of the central star. Since the ratio $\gamma = \tau_{\rm Sda}/\tau_{\rm Sd}$ is calculated from observational data ($n_{\rm e}$ and $n_{\rm e}^2\,V$) with each $N_{\rm U}(*)$, we can find a value, $N_{\rm Ui}(*)$, which gives $\gamma = 1$ with the use of Eqs. (6)−(8). Trials were made for the sources IRS1(A/2), IRS1(B), IRS1(L) and IRS3, with the radio data of Cols. 6 and 7 in Table 5, as shown in Fig. 7. Then, the obtained $N_{\rm Ui}(*)$ are marked in Figs. 7c and 7d. These trials are in contrast with the way in which the internal $L_{*{\rm i}}$ and $N_{\rm U}(*)$ were estimated from the intrinsic luminosity and the effective solid angle of the IR sources with Eqs. (1)−(3). In Figs. 7c and 7d we see that for the regions of IRS2(L) and IRS3, reasonable $N_{\rm Ui}(*)$ can be found easily around each $N_{\rm U}(*)$ of the Col. 4 in Table 5. This means that, for the gas with standard dust content, $N_{\rm U}(*)$ determined from the luminosity of the IR sources can be accepted (within a factor of 2) as a working model of the study. But for the regions IRS1(A/2) and IRS1(B) (Figs. 7a and b), it seems rather difficult to find reasonable $N_{\rm Ui}(*)$ which satisfy $\gamma \simeq 1$ as the gas with standard dust content such as $\tau_{\rm Sd}/\tau_{\rm SH} = 1/3100$. We see a feature of a general dependence of $N_{\rm U}(*)$ on γ in each of Figs. 7. We know that there must be gas of $\gamma \neq 1$, as well as of $\gamma = 1$, in compact HII regions.

3.2. Ratio of dust mass density to hydrogen mass density

The gas of dust content other than $\gamma \simeq 1$ will be considered here. Following the extinction criterion by Spitzer (1978; Eqs. (7)−(26)) again, the ratio of dust mass density, $\rho_{\rm da}$, to hydrogen mass density, $\rho_{\rm H}$, in the gas will be approximately given by

$$\rho_{\rm da}/\rho_{\rm H} \simeq 0.6\times10^{-2}\gamma. \tag{9}$$

We have studied Eq. (9) in another way, using only the extinction criterion of Eq. (5). From equations, $\tau_{\rm Sd} = Q_{\rm abs}\pi a^2\,n_{\rm d}\,r_{\rm S}$ (a: grain radius, $n_{\rm d}$; grain number density) and $\tau_{\rm SH} = s\,n_{\rm H}\,r_{\rm S}$, then $(\tau_{\rm Sd}/\tau_{\rm SH})_{\rm S} = (n_{\rm d}/n_{\rm H})_{\rm S}(Q_{\rm abs}\pi a^2/s) = 1/3100$, where the subscript "s" means the standard gas. $(\rho_{\rm da}/\rho_{\rm H})_{\rm S} = (n_{\rm d}/n_{\rm H})_{\rm S}(m_{\rm a}/m_{\rm p}) = 4.86\times10^3\,a({\rm cm})/Q_{\rm abs}$ ($m_{\rm a}$: mass of a grain $3\times4\pi a^3/3$ g, Spitzer p162), ($m_{\rm p}$: mass of a proton 1.67×10^{-24} g). When we write $\rho_{\rm da}/\rho_{\rm H} \simeq (\rho_{\rm da}/\rho_{\rm H})_{\rm S}(\tau_{\rm Sda}/\tau_{\rm Sd})$

Table 5. $\tau_{\rm Sda}$, $\tau_{\rm Sd}$, and ionization parameters. (4): Number of ionizing photon emissions per second from the central star (Panagia 1973; Spitzer 1978). (5): Radius of ionized sphere (Akabane et al. 1992). (6): Volume emission measure as $V = (4\pi/3)r_{\rm i}^3$. (7): Electron density of compact HII regions (Akabane et al. 1992). (8): $(r_{\rm i}/r_{\rm s})^3$ = the fraction of ionizing photons which is absorbed by H atoms rather than by dust in the entire ionized region (Spitzer 1978). $r_{\rm S}$ is the Strömgren sphere radius. (9): Dust opacity for the actual gas. (10): Dust opacity for the apparent gas of the standard dust content. (11): Dust opacity ratio γ (= $\tau_{\rm Sda}/\tau_{\rm Sd}$). (12): $\xi = (\tau_{\rm Sda}/\tau_{\rm Sd})/[\{N_{\rm U}(*)(\rm s^{-1})\}]^{-1/2}$. (see the text)

Sources	Central star			HII			Dust opacity out to $r_{\rm S}$ (Spitzer 1978)				
(1)	(2)	(3)	(4)	(5)	(6)	(7)	(8)	(9)	(10)	(11)	(12)
NGC 7538	Spectral	$L_{*\rm i}/L_\odot$	$N_{\rm U}(*)$	$r_{\rm i}$	$n_{\rm e}^2\,V$	$n_{\rm e}$	$r_{\rm i}/r_{\rm S}$	$\tau_{\rm Sda}$	$\tau_{\rm Sd}$	$\tau_{\rm Sda}/\tau_{\rm Sd}$	$\xi\times10^{-7}$
(N)	type		($\rm s^{-1}$)	(cm)	($\rm cm^{-3}$)	($\rm cm^{-3}$)					
IRS1(A/2)	$\sim$O7 × 1	9.6×10^4	3.0×10^{48}	1.3×10^{16}	0.85×10^{60}	2.2×10^5	0.503	5.4	14.4	3.75×10^{-1}	1.40
IRS1(B)	$\sim$O6 × 1	3.2×10^5	1.5×10^{49}	3.8×10^{15}	7.2×10^{60}	4.9×10^6	0.599	3.3	69.1	4.78×10^{-2}	1.38
IRS2(L)	$\sim$O4.5 × 1	8.5×10^5	5.1×10^{49}	1.7×10^{17}	3.2×10^{60}	7.7×10^3	0.304	14.0	12.1	1.15	1.29
IRS3	$\sim$B0 × 1	3.3×10^4	1.7×10^{47}	1.3×10^{16}	5.3×10^{58}	7.1×10^4	0.519	5.0	3.78	1.32	1.18

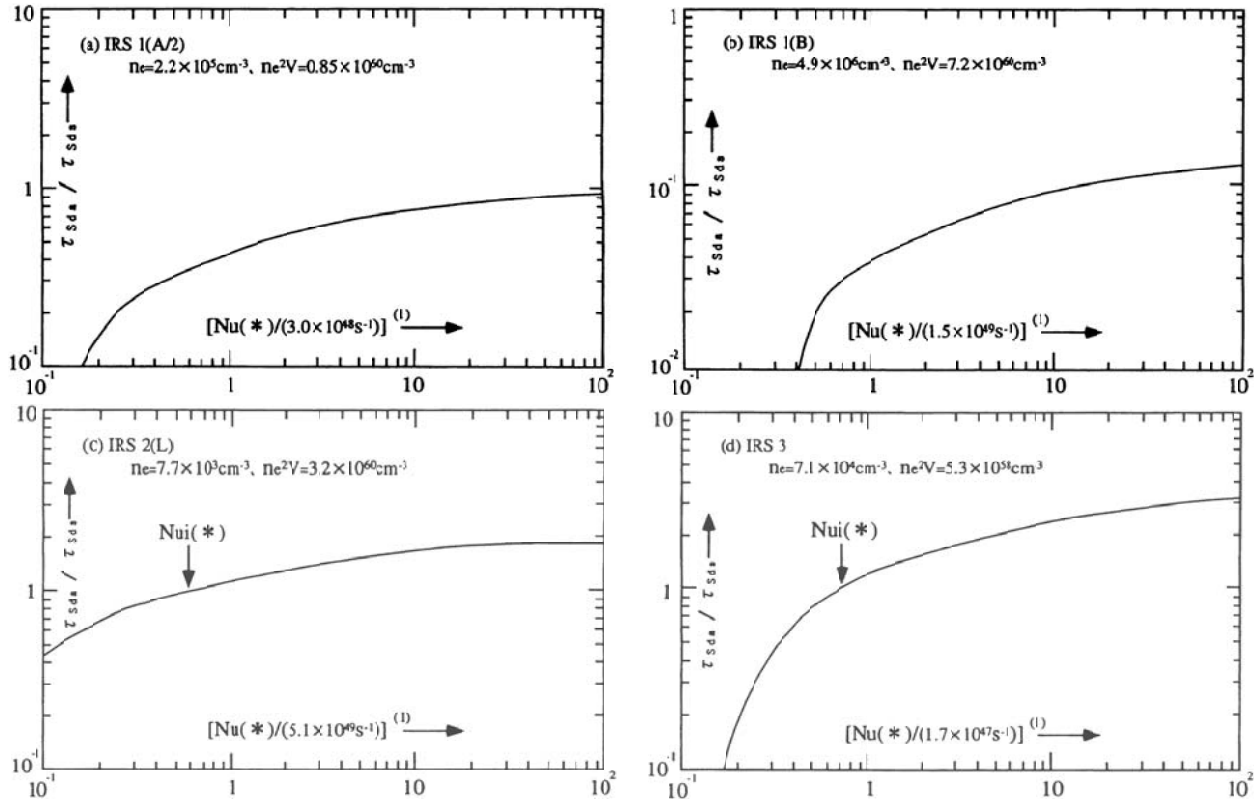

Fig. 7. Relative dust content, $(\tau_{\rm Sda}/\tau_{\rm Sd})$, against the stellar ionizing photon, $N_{\rm U}(*)$, from Eqs. (6)−(8) with the use of observed data $n_{\rm e}^2\,V$ and $n_{\rm e}$ of the Cols. (6) and (7) respectively in Table 5. Figures 7a−d are for the sources IRS1(A/2), IRS1(B), IRS2(L), and IRS3 respectively. (1): $N_{\rm U}(*)$ is normalized with each assumed one in the Col. (4) of the Table 5.

instead of Eq. (9), $(\rho_{\rm da}/\rho_{\rm H})_{\rm S}$ gives the mass density ratio of dust and hydrogen of the standard gas. $(\rho_{\rm da}/\rho_{\rm H})_{\rm S}$ is proportional to $a({\rm cm})/Q_{\rm abs}$ in the above equations, and is estimated as $\sim4.8\times10^{-3}$ and $\sim4.8\times10^{-2}$ for model grains of $a = 0.01\,\mu$m and $a = 0.1\,\mu$m of the astronomical silicate (Draine 1985), respectively. We see that the former ($a = 0.01\,\mu$m) seems more plausible than the latter ($a = 0.1\,\mu$m) for Eq. (9) in which the dust mass ratio for the standard gas is derived from the extinction criterion (Spitzer 1978).

3.3. Relative dust mass content, γ, and ionizing photon rate

We see a good constancy of $\xi = \gamma/\{N_{\rm U}(*)/4\pi r_{\rm i}^2\}^{-1/2}$ in Col. 12 of Table 5, as also seen in Fig. 8. Filled circles in Fig. 8 are the plots of γ as calculated in Eqs. (6)−(8) against each $\{N_{\rm U}(*)/4\pi r_{\rm i}^2\}^{-1/2}$ from the observational data in Table 5. The specified values of $\Omega_{\rm e}/\Omega_0$ of Col. 8 in Table 4 were used to find the stellar luminosities of Eq. (3). The upper side error

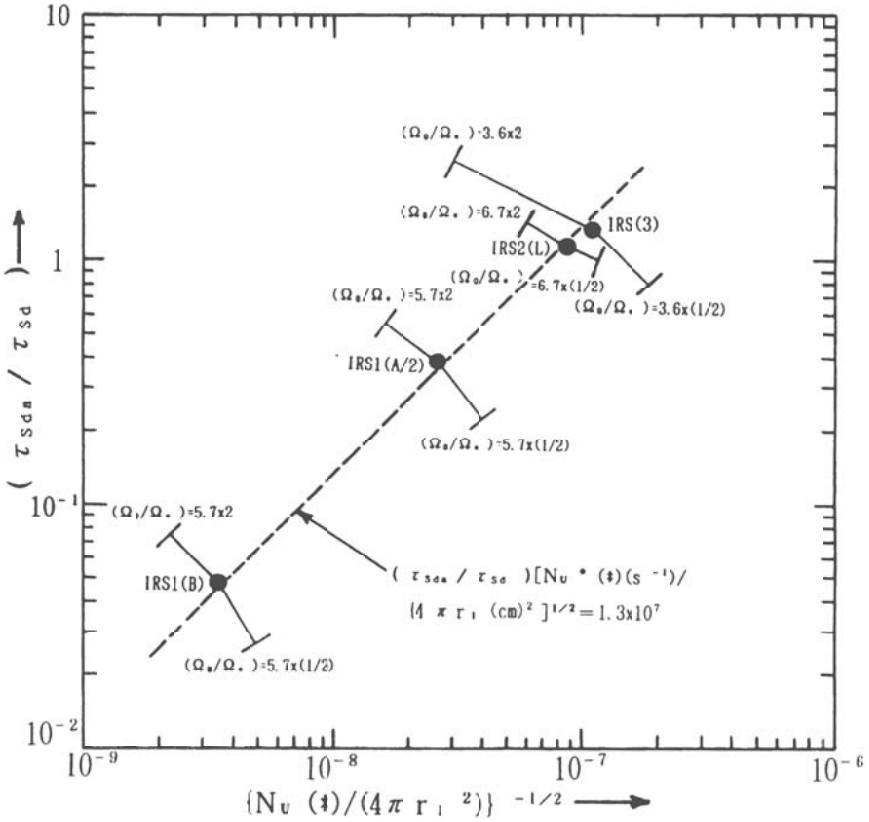

Fig. 8. Relative dust content γ $\{=(\tau_{\rm Sda}/\tau_{\rm Sd})\}$ against $\{N_{\rm U(*)}/(4\pi r_{\rm i}^2)\}^{-1/2}$ ($\rm s^{1/2}\,cm$) for the compact HII regions IRS1(A/2), IRS1(B), IRS2(L), and IRS3 in the NGC 7538(N).

limits in Fig. 8 show the calculated γ for each $\{N_{\rm U}(*)/4\pi r_{\rm i}^2\}^{-1/2}$ assuming two times larger $\Omega_0/\Omega_{\rm e}$ in Eq. (3) and the corresponding $N_{\rm U}(*)$ but with the constants of the derived $L_{\rm IRSi}$ in Table 4 and the observed $r_{\rm i}$, $n_{\rm e}^2\,V$, and $n_{\rm e}$ in Table 5. This corresponds to the change of the location of IR source from $0.5\,r_{\rm i}$ to $0.7\,r_{\rm i}$. The lower error limits are estimated using the same procedure, but a half of $\Omega_0/\Omega_{\rm e}$ in Eq. (3) was applied to each source, and this corresponds to the change of the location of the IR source from $0.5\,r_{\rm i}$ to $0.35\,r_{\rm i}$. A widely scattered γ with $\{N_{\rm U}(*)/4\pi r_{\rm i}^2\}^{-1/2}$ arises from the uncertainties of $\Omega_0/\Omega_{\rm e}$ in Eq. (3). Then we assumed that the ambiguity of the location of each IR source is limited as $\sim 0.3 r_{\rm i} < r_{\rm IRS} <\sim 0.7 r_{\rm i}$ if the sources are in each ionized sphere, with the accuracy of a factor of about 2 and 10 for γ and $N_{\rm U}(*)$, respectively. In this situation, a multiple body structure of the IR source having the total solid angle equal to each $\Omega_{\rm e}$ should be considered. The ambiguity of the shared luminosities to the components of IRS1(A/2)×2 and IRS1(B) does not yield a large error for the γ compared to those from the uncertainty of $\Omega_0/\Omega_{\rm e}$ in Eq. (3), because of a relatively shallow dependence of γ on $N_{\rm U}(*)$ as in Figs. 7a and 7b.

In Fig. 8, a nearly standard dust content can be seen in the regions of IRS2(L) and IRS3, but a depletion of dust content (cf. Eq. (9)) is present for the regions of IRS1(A/2) and IRS1(B) as also suggested in Figs. 7a and 7b. The dashed straight line in Fig. 8 is for $\gamma\{N_{\rm U}(*)/4\pi r_{\rm i}^2\}^{1/2} = 1.3\times10^7(\rm s^{-1/2}\,cm^{-1})$, as the mean value of ξ of the Col. 12 in Table 5.

3.4. Dust content in compact HII regions

In Fig. 8, we see a good correlation between the relative dust content, γ, and the stellar ionizing photon flux density, $N_{\rm U}(*)/(4\pi r_{\rm i}^2)$. In this section, we try the same treatment as in Sect. 3.3 for some of the compact or ultra-compact HII regions catalogued by the VLA, although the estimate of $N_{\rm c}^*$ $\{=N_{\rm U}(*)\}$ from $N_{\rm c}$ $\{=N_{\rm u}(\rm radio)\}$ was made in a way different from ours. The catalogued data by Wood & Churchwell (1989, hereafter WC) and Kurts et al. (1994, hereafter KWC) are used for this study. 14 compact or ultra-compact HII regions which are spherical and fairly isolated from the nearby complex were selected. We have used their $N_{\rm c}^*$ for our $N_{\rm U}(*)$ of Fig. 8, and the diameter of the sphere (pc) is $2\,r_{\rm i}$(cm). The calculated γ from their listed data are plotted against $(N_{\rm c}^*/4\pi r_{\rm i}^2)^{-1/2}$ in Fig. 9. The plots in Fig. 9 show a similar trend to that in Fig. 8, but the correlation that $\gamma(N_{\rm c}^*/4\pi r_{\rm i}^2)^{1/2}$ = constant is not clear. A fitted straight line of $\gamma\,(N_{\rm c}^*/4\pi r_{\rm i}^2)^{0.721/2} = 3.18\times10^5$ with the correlation coefficient of $R_{\rm c} = 0.851$ is shown in Fig. 9. However, a very wide range of $(N_{\rm c}^*/4\pi r_{\rm i}^2)^{-1/2}$ calculated from their data yields a wide range of $\gamma \sim 10^{-1}$ to 15. Compact HII regions which are used in Fig. 9 numbered from (1) to (14) are listed in the figure's notes. The spectral type of the central star is also added to each plot in the figure to see its dependence on γ.

From the Eqs. (6)–(8) γ is given as

$$\gamma = [(\tau_{\rm Sda} f^{1/3})/(1/3100)]\,[(4/3)\pi\alpha_{\rm B}]\,[r_{\rm i}/N_{\rm U}(\rm radio)]^{1/2}, \quad (10)$$

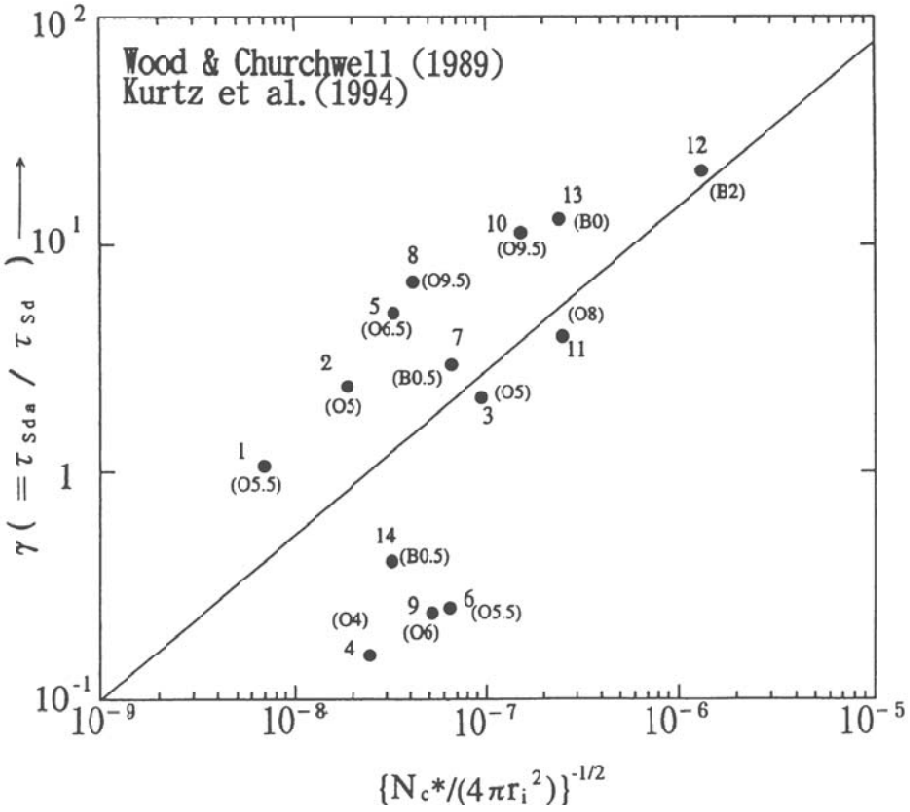

Fig. 9. Relative dust content γ {$= (\tau_{Sda}/\tau_{Sd})$} of the 14 compact HII regions from the catalogued data by Wood & Churchwell (1989) and Kurtz et al. (1994) against their $\{N_c^*/(4\pi r_i^2)\}^{-1/2}$, with r_i(cm) of {linear diameter (pc)}/2.

Notes:Adopted sources from WC and KCW,

	Source	Sp. type	$1-f_d^{(i)}$		Source	Sp. type	$1-f_d^{(i)}$
(1)	G15.04−0.68	O5.5	0.01	(8)	G76.383−0.621	O9.5	0.01
(2)	G23.46−0.20	O5	0.01	(9)	G133.947+1.064	O6	0.09
(3)	G25.72+0.05	O5	0.01	(10)	G138.295+1.555	O9.5	0.01
(4)	G45.07+0.13	O4	0.06	(11)	G139.909+0.197	O8	0.01
(5)	G54.10−0.06[(ii)]	O6.5	0.01	(12)	G189.030+0.784[(ii)]	B2	0.05
(6)	G28.200−0.049	O5.5	0.07	(13)	G189.876+0.516[(ii)]	B0	0.01
(7)	G60.884−0.128	O8.5	0.02	(14)	G206.543−16.347	B0.5	0.01

(i): $1-f_d = (N_c'/N_c^*)$, by (WC) and (KWC), but the excitation parameter U was used for the estimation of γ $(= \tau_{Sda}/\tau_{Sd})$. (ii): For the unresolved sources (5), (12), and (13) in the list, the maximum linear diameter and the minimum n_e of each source were adopted.

where $f = N_U(\text{radio})/N_U(*)$ or $= (r_i/r_s)^3$, and τ_{Sda} also is a function of f, $\tau_{Sda}(y_i = f^{1/3})$, as given by Eqs. (7) and (8). Then we have the simple equation (Akabane & Kuno 2002)

$$\gamma = G(f)[r_i/N_U(\text{radio})]^{1/2}, \quad (11)$$

where $G(f)$ is a function of f; $G(f) = [\tau_{Sda}(f)f^{1/3}/(1/3100)][(4/3)\pi\alpha_B]$. We see that γ is proportional to $[r_i/N_U(\text{radio})]^{1/2}$ for a fixed value of f. But in the γ vs. $[r_i/N_U(\text{radio})]^{1/2}$ diagram the plots of observed results will be scattered around a general trend (if any) for each value of $G(f)$. Akabane & Kuno (2002) discussed, in their Fig. 4, the role of $G(f)$ of Eq. (11) according to each value of f in the range 0.001 to 0.5.

Chini et al. (1987) pointed out that for very luminous stars, the inner region often contains a dust-depleted HII region. We see a faint tendency in Fig. 9 such that intense stars, as O8<, appear with relatively small γ.

4. Discussion

4.1. τ_{Sda} with the astronomical silicate

We evaluated τ_{Sda} for the compact HII regions from Eqs. (5)−(8) following Spitzer (1978). The results are listed in Col. 9 of Table 5. On the contrary, we calculate τ_{Sda} with the appropriate model of dust grains, e.g. astronomical silicate (Draine 1985). We denote the calculated τ_{Sda} by τ_{Sda}(c). For

Table 6. $\tau_{\rm Sda}$ compared with $\tau_{\rm Sda}$(c) as defined by $\kappa_{\rm d} r_{\rm S}$, $\kappa_{\rm d}$ of the ionizing photon dust absorption coefficient along the Strömgren sphere radius, $r_{\rm S}$. Column (4): actual dust-mass density in the region $r < r_{\rm i}$ as $\rho_{\rm da} = \gamma \times 0.6 \times 10^{-2}\, m_{\rm p}\, n_{\rm H}$ from Eq. (9), with $m_{\rm p}$ (=1.67×10^{-24} g) of the mass of a hydrogen atom and $n_{\rm H}$ of the number density of hydrogen atom, and $n_{\rm H} = n_{\rm e}$. Column (5): dust-absorption coefficient for the ionizing photon ignoring scattering effects as $\kappa_{\rm d}$ (at $\lambda = 0.1\,\mu$m) $\simeq Q_{\rm abs} \times \pi a^2 n_{\rm da}$ with the grain radius a of 0.01 μm, $Q_{\rm abs}$ of about 1.0 from Draine's astronomical silicate, and $n_{\rm da}$ (=$\rho_{\rm da}/m_{\rm a}$) of the grain-number density of the region. We assumed mass of a grain as $m_{\rm a}$ {=3 g cm^{-3} × $(4\pi/3)(0.01\,\mu{\rm m})^3 = 1.26 \times 10^{-17}$ g} using the mass density of a grain of about 3 g cm^{-3} (Spitzer 1978, p.162). Column (8): calculated ionizing photon opacity for the grain of Draine's astronomical silicate of $a = 0.01\,\mu$m as $\kappa_{\rm d}\, r_{\rm S}$ with $r_{\rm S}$ from $r_{\rm i}$ and $r_{\rm i}/r_{\rm S}$ of Cols. (6) and (7) respectively. Column (9): estimated opacity as in Col. (9) of Table 5 from Spitzer's formulae of Eqs. (6)−(8) in the text.

(1)	(2)	(3)	(4)	(5)	(6)	(7)	(8)	(9)
NGC 7538	$n_{\rm e}$	γ	$\rho_{\rm da}$	$\kappa_{\rm d}$	$r_{\rm i}$	$r_{\rm i}/r_{\rm S}$	$\tau_{\rm Sda}$(c)	$\tau_{\rm Sda}$
(N)	(obs.)	(obs.)	(calc.)	(calc.)	(obs.)	(obs.)	(calc.)	(obs.)
	(cm^{-3})		(g cm^{-3})	(cm^{-1})	(cm)	(with $N_{\rm U}^{*}$)		
IRS1(A/2)	2.2×10^{5}	3.8×10^{-1}	8.3×10^{-22}	2.1×10^{-16}	1.3×10^{16}	0.503	5.3	5.4
IRS1(B)	4.9×10^{6}	4.8×10^{-2}	2.3×10^{-21}	6.0×10^{-16}	3.8×10^{15}	0.599	3.8	3.3
IRS2(l)	7.7×10^{3}	1.15	8.9×10^{-23}	2.2×10^{-17}	1.7×10^{17}	0.304	12.2	14.0
IRS3	7.1×10^{4}	1.32	9.4×10^{-22}	2.4×10^{-16}	1.3×10^{16}	0.519	5.9	5.0

Table 7. Dust feature around the ionized sphere and a speculated structure of the IR source. Column (4): dust mass density of Willner's absorption layer as assumed to be homogeneously extended throughout the FIR(2 mm) clumpy dust cloud (cf. Fig. 6). Column (5): radius of IR source, from observed $\Omega_{\rm e}$ in Table 2 and the adopted distance R = (2.8 kpc) to the source. Column (6): number density of the dust grain in the IR source, derived from the assumption that τ(IRS at $\lambda = \lambda_{\rm peak}$) ≡ 10 with $a = 0.01\,\mu$m silicate grains (Draine 1985). Column (7): dust mass density of the IR source derived by 1.26×10^{-17} g × $n_{\rm dI}$(IRS). Column (8): mass of the IR source, material mass density of the silicate grain assumed as 3 g cm^{-3} (Spitzer 1978, p.162). Column (9): estimated dust mass when volume $(4\pi/3)r_{\rm i}^3$ was filled by $\rho_{\rm dF}$ ($\simeq 4.6 \times 10^{-20}$ g cm^{-3}) of the mass density which is homogenized for the outside clumpy FIR(2 mm) dust grain in the envelope of the ionized sphere (Akabane et al. 2001) (cf. Fig. 6). (∗): Opacity of the surrounding Willner's dust layer at $\lambda = 9.7\,\mu$m was assumed to be roughly 2.0, avoiding the direction to the observer.

(1)	(2)	(3)	(4)	(5)	(6)	(7)	(8)	(9)
Source	$r_{\rm i}$	$\rho_{\rm da}$	$\rho_{\rm AS}$	$a_{\rm I}$(IRS)	$n_{\rm dI}$(IRS)	$\rho_{\rm dI}$(IRS)	$M_{\rm d}$(IRS)	$M_{\rm dF}$
NGC 7538		$r < r_{\rm i}$	$r \geq r_{\rm i}$	(single body)	(single body)	(single body)		$\rho_{\rm dF}(4\pi/3)r_{\rm i}^3$
(N)	(cm)	(g cm^{-3})	(g cm^{-3})	(cm)	(cm^{-3})	(g cm^{-3})	(g)	(g)
				(AU)			($M_{\odot}$)	
IRS1(A/2)	1.3×10^{16}	8.3×10^{-22}	1.2×10^{-21}	5.4×10^{15}	$\geq 1.1 \times 10^{-1}$	1.4×10^{-18}	1.3×10^{30}	0.43×10^{30}
				3.6×10^{2}			0.66×10^{-3}	
IRS2(L)	1.7×10^{17}	8.9×10^{-23}	$^{(*)}7.9 \times 10^{-22}$	6.8×10^{16}	$\geq 3.6 \times 10^{-1}$	4.5×10^{-18}	7.8×10^{33}	0.95×10^{33}
				4.5×10^{3}			3.9	
IRS3	1.3×10^{16}	9.4×10^{-22}	3.0×10^{-22}	6.6×10^{15}	$\geq 1.4 \times 10^{-1}$	1.8×10^{-18}	2.9×10^{30}	0.43×10^{30}
				4.4×10^{2}			1.4×10^{-3}	

this, we calculated $\rho_{\rm da}$ from Eq. (9) and $\kappa_{\rm d}$ from the Draine silicate grain of radius 0.01 μm as in Table 6, combin with the observed $n_{\rm e}$, γ, $r_{\rm i}$, and $r_{\rm i}/r_{\rm s}$ for each region, listed in Table 5. Then we can compare $\tau_{\rm Sda}$(c) with $\tau_{\rm Sda}$ as in Cols. 8 and 9 of Table 6. We see that both are in good agreement with each other for each region. We know that there certainly exist some specified dust grains which satisfy the theoretical criterion for dust extinction, as in Eqs. (5) and (9) by Spitzer (1978) in compact HII regions. Dust grains with the radius $a = 0.1\,\mu$m give $\rho_{\rm da}/\rho_{\rm H} \simeq 4.8 \times 10^{-2}\gamma$ (cf. Sect. 3.2), providing almost the same $\tau_{\rm Sda}$(c) as Col. 8 in Table 6. However, we used here a restricted astronomical silicate grain of $a = 0.01\,\mu$m for which we can expect $\rho_{\rm da} = \gamma \times 0.6 \times 10^{-2} m_{\rm p} n_{\rm H}$ for Eq. (9) as introduced by Spitzer (1978, Eqs. (7)−(26)) (cf. Sect. 3.2).

4.2. Dust and IR source in the ionized sphere

A simplified dust structure of the IR source and its environment will be studied here. For this, we examined Draine's astronomical silicate grains with a radius of 0.01 μm (Draine 1985) for an assumed dust model. The absorption layer in Willner (1976) is assumed to be widely but homogeneously extended within the far outer FIR clumpy dust (cf. Fig. 6). We assumed also

that this Willner's dust and the massive neutral hydrogen can balance the internal ionization front at the boundary of each HII source.

IRS2(L) was identified as the dust-depleted region of NGC 7538(N), the void structure, by Chini et al. (1986). They presented the surrounding feature with the density discontinuity of dust, even though no Willner's absorption dip was observed as in Fig. 3. The density discontinuity of dust in NGC 7538(N) seen by Chini et al. (1986) would appear at around the radius of the ionized sphere of the IRS2(L). $a_{\rm I}$(IRS) in Table 7 is the radius of each IR source. $n_{\rm dI}$(IRS) in Table 7 is the number density of the dust grain in each IR source derived, assuming that τ (IRS at $\lambda = \lambda_{\rm peak}$) = 10 with $a = 0.01\,\mu$m silicate grains (Draine 1985). $\rho_{\rm dI}$(IRS) in Table 7 is the dust mass density in each IR source derived by $1.26 \times 10^{-17} \times n_{\rm dI}$(IRS). These are considered for a single body of each IR source, and then a clumped multi-body model of the IR source would give appreciably larger values of $n_{\rm dI}$(IRS) and $\rho_{\rm dI}$(IRS) than those in the table. The opacity at the peak of $B_\nu(110\,{\rm K})\,\Omega_{\rm e}$ for IRS2(L) in Fig. 3 was assumed as $\tau_\lambda({\rm P}) \leq 10$ for the calculation of the mass of the IRS2(L), $M_{\rm d}$(IRS), in Col. 8 of Table 7. In the case of $\tau_\lambda({\rm P}) \gg 10$ and with the opacity index β of about 2.0, there is a possibility that the red side wing of $B_\lambda(110\,{\rm K})\,\Omega_{\rm e}$ of the peak intensity of $3.0 \times 10^{-23}\,{\rm W\,m^{-2}\,Hz^{-1}}$ covers mm to submm observational data (e.g. Akabane et al. 2001). But almost no such confusion has been observed in these wavelength regions so far, so we assumed $\tau_\lambda({\rm P}) \leq 10$ for the IRS2(L). We assumed also $\tau_\lambda({\rm P}) \sim 10$ for sources of IRS1 and IRS3. $M_{\rm dF}$ in the Col. 9 of Table 7 is the assumed mass of dust in the ionized sphere, when its volume $4\pi r_{\rm i}^3/3$ was filled with the neighboring homogenized FIR dust with a mean dust mass density of $\rho_{\rm dF}$ as $\sim 4.6 \times 10^{-20}\,{\rm g\,cm^{-3}}$ (Akabane et al. 1992). We see that the total mass of the IR source, $M_{\rm d}$(IRS) in Table 7, coincides in order with $M_{\rm dF}$, and then we speculate that the dust depleted region, the space of the inner region given as $r < 2 \times 10^{17}$ cm by Chini et al. (1986), will be due to the accretion of dust to the IR source, rather than to the evaporation of the dust grain with the radiation from the central star.

5. Summary

(1) Fitting models to a IR source as the underlying black body behind the silicate absorption layer (Willner 1977) revealed (i) black body temperature $T_{\rm IRS}$, effective emitting area $\Omega_{\rm e}$, and total luminosity $L_{\rm IRSi}$ of the IR sources; (ii) stellar luminosity $L_{\rm i*}$, and then stellar UV photons $N_{\rm U}(*)$ which are estimated from $\Omega_{\rm e}$ of the extent of the IR source and Ω_0 of that of the ionized sphere; and (iii) grain temperature $T_{\rm AS}$ lower than ~70 K, and the central distance of $\sim 2 \times 10^{17}$ cm for Willner's absorption layer.

(2) The relative dust mass ratio $\gamma(=\tau_{\rm Sda}/\tau_{\rm Sd})$ was introduced following Spitzer (1978), and relationship $\gamma\{N_{\rm U}(*)/4\pi r_{\rm i}^2\}^{1/2} = 1.3 \times 10^7 ({\rm s^{-1/2}\,cm^{-1}})$, was obtained for the 4 compact HII regions in NGC 7538(N).

(3) A range of the relative dust mass ratios of $\sim 0.1 < \gamma < 15$ was roughly estimated for compact or ultra-compact HII regions.

(4) Spitzer's theoretical result of $\tau_{\rm Sda}$ obtained in this study was investigated with an actual dust-grain model. The astronomical silicate grain of $a = 0.01\,\mu$m (Draine 1985) in each region gives a fairly good $\tau_{\rm Sda}$(c), very close to the theoretical $\tau_{\rm Sda}$, although the scattering effect was ignored.

(5) If NGC 7538(N) (Chini et al. 1986) is identified as the ionized sphere of the IRS2(L) in the region, the boundary of the dust-depleted cavity will be balanced by Willner's dust layer and the neutral hydrogen.

(6) The dust-depleted region, in which the IR sources are assumed to be located, was studied, assuming Draine's astronomical silicate grain of $a = 0.01\,\mu$m, and the mass of each IR source was estimated. The mass of the IRS2(L), $M_{\rm d}$(IRS2L), was given as $M_{\rm d}({\rm IRS2}) = 1 \sim 4\,M_\odot$ as a working model.

Acknowledgements. We are very grateful to Professors N. Nakai, and M. Inoue of the Nobeyama Radio Observatory for their kind consideration and comments. Useful discussions were had with Drs. H. Matsuo, M. Momose, and O. Kameya. Prof. Y. Nakada helped us with fundamental knowledge of the interstellar dust. Prof. W. Unno kindly read the manuscript with critical comments. A part of the work by one of authors (K.A.) was supported by the Research Program of the A. E. S. Corporation Ltd., Tsukuba Japan. Miss C. Yoda is also cordially thanked for drafting tables and figures for this study.

References

Akabane, K., Tsunekawa, S., Inoue, M., et al. 1992, PASJ, 44, 421
Akabane, K., Matsuo, H., Kuno, N., & Sugitani, K. 2001, PASJ, 53, 821
Akabane, K., & Kuno, N. 2002, Proc. 8th IAU Asian Pacific Regional Meeting, Tokyo, Vol. II, 121
Beckwith, S. V. W., Evans, II., N. J., Becklin, E. E., & Neugebauer, G. 1976, ApJ, 208, 390
Bloomer, J. D., Watson, D. M., Pipher, J. L., Forrest, W. J., & All, B. 1998, ApJ, 506, 727
Campbell, B. 1984, ApJ, 282, L27
Campbell, B., & Persson, S. E. 1988, AJ, 95, 1185
Chini, R., Krugel, E., & Kreysa, E. 1986, A&A, 167, 315
Chini, R., Krugel, E., & Wargau, W. 1987, A&A, 181, 378
Churchwell, E., Wolfire, M. G., & Wood, D. O. S. 1990, ApJ, 354, 247
Draine, B. T. 1985, ApJS, 57, 585
De Pree, C. D., Mehringer, D. M., & Goss, W. M. 1997, ApJ, 482, 307
Dreher, J. W., Johnston, K. J., Welch, W. J., & Walker, R. C. 1984, ApJ, 283, 632
Garay, G., Rodoriguez, L. F., Moran, J. M., & Churchwell, E. 1993, ApJ, 418, 368
Garay, G., & Lizano, S. 1999, PASP, 111, 1049
Gaume, R. A., Claussen, M. J., De Pree, W. M., & Mehringer, D. M. 1995a, ApJ, 449, 663
Gaume, R. A., Goss, W. M., Dickel, H. R., Wilson, T. L., & Johnston, K. J. 1995b, ApJ, 438, 776
Gillet, F. C., Forrest, W. J., Merill, K. M., Capps, R. W., & Soifer, B. T. 1975, ApJ, 200, 609
Hackwell, J. A., Grasdalen, G. L., & Gehrz, R. D. 1982, ApJ, 252, 250

Kameya, O., Hirano, N., Kawabe, R., & Campbell, B. 1991, in Proc. 7th Manchester Astronomical Conf. on Molecular Cloud, ed. R. A. James, & T. J. Miller (Cambridge: Cambridge University press), 111
Kameya, O., Hasegawa, T. I., Hirano, N., & Takakubo, K. 1989, ApJ, 339, 222
Kawabe, R., Suzuki, M., Hirano, N., et al. 1992, PASJ, 44, 435
Kurtz, S., Churchwell, E., & Wood, D. O. S. 1994, ApJS, 91, 659
Martin, A. H. M. 1973, MNRAS, 63, 141
Momose, M., Tamura, O., Kameya, O., et al. 2001, ApJ, 555, 855
Panagia, N. 1973, AJ, 78, 929
Petrosian, V., Silk, J., & Field, G. B. 1972, ApJ, 177, L69
Scoville, N. Z., Sargent, A. I., Sandars, D. B., et al. 1986, ApJ, 303, 416
Spitzer, L. JR. 1978, Physical Processes in the Interstellar Medium (New York: John Wiley and Sons, Inc.), 103
Thronson, H. A., & Harper, D. A. 1979, ApJ, 230, 133
Vacca, W. D., Garmany, C. D., & Shull, J. M. 1996, 460, 914
Werner, M. W., Becklin, E. E., Gatley, I., et al. 1979, MNRAS, 188, 463
Willner, S. P. 1976, ApJ, 296, 728
Wood, D. O. S., Handa, T., Fukui, Y., et al. 1988, ApJ, 326, 884
Wood, D. O. S., & Churchwell, E. 1989, ApJS, 69, 831
Wynn-Williams, C. G., Becklin, E. E., & Neugebauer, G. 1972, MNRAS, 160, 1
Wynn-Williams, C. G., Werner, M. W., & Wilson, W. J. 1974, ApJ, 187, 41
Wynn-Williams, C. G., Becklin, E. E., & Neugebauer, G. 1974, ApJ, 187, 473
Wynn-Williams, C. G., & Becklin, E. E. 1974, PASP, 86, 5